Dynamics of silica glass: two-level tunnelling states and low-energy floppy modes

2000 J. Phys.: Condens. Matter 12 8041

(http://iopscience.iop.org/0953-8984/12/37/304)

J. Phys.: Condens. Matter **12** (2000) 8041–8064. Printed in the UK PII: S0953-8984(00)14286-9

Dynamics of silica glass: two-level tunnelling states and low-energy floppy modes

Kostya O Trachenko†‡, Martin T Dove†§‖, Mark J Harris§ and Volker Heine‡

† Mineral Physics Group, Department of Earth Sciences, University of Cambridge, Downing Street, Cambridge CB2 3EQ, UK

‡ Cavendish Laboratory, University of Cambridge, Madingley Road, Cambridge CB3 0HE, UK

§ ISIS Facility, Rutherford Appleton Laboratory, Chilton, Didcot, Oxfordshire OX11 0QX, UK

E-mail: martin@esc.cam.ac.uk (M T Dove)

Received 24 May 2000

Abstract. We present the results of a computational study of the low-energy dynamics of silica glass. Molecular dynamics simulation results show that parts of the glass structure can undergo large cooperative reorientations of SiO_4 tetrahedra. These motions involve reorientations of about 30 tetrahedra with an energy barrier of about 0.06 eV. We relate these motions to the presence of double-well potentials which give rise to two-level tunnelling states in the model, thereby providing the mechanism for the anomalous low-temperature thermal properties of glasses. Simulation of larger structures of silica glass shows that jump events become more frequent and uncorrelated with each other. In addition to studying the flexibility of silica glass in terms of the large tetrahedral rearrangements, we also address the flexibility of silica glass in terms of its ability to sustain low-ω floppy modes. The latter part of the study is supported by inelastic neutron scattering data, and we compare experimental and calculated dynamic structure factors in the energy range 0–10 meV and scattering vector range 0–8 Å^{-1}. By applying the analysis of the rigid-unit-mode model as initially developed for crystalline silicates to structures of silica glass we find that silica glass is surprisingly similar to its corresponding crystalline phases in its ability to support low-ω floppy modes. The same conclusion follows from the comparison of calculated vibrational densities of states of silica glass and its crystalline phases, and is borne out in the inelastic neutron scattering data.

1. Introduction

The low-energy vibrational dynamics of glasses has been the subject of intensive studies in recent years. The presence of excess, as compared to crystalline phases, low-energy vibrational states can explain anomalous low-temperature thermal properties of glasses [1]. This is done in the phenomenological model introduced by Anderson, Halperin, and Varma [2] and Phillips [3], which postulates the existence of localized low-energy excitations in glasses. For a given temperature, the participating atoms are those for which the value of the energy barrier is comparable with $k_B T$. The tunnelling between minima of double-well potentials with such energy barriers is then introduced which is the major point of the model, thus giving rise to two-level tunnelling states.

However, it has been difficult to pinpoint the existence of double-well potentials in glasses clearly, which has contributed to the growth of the literature doubting their existence and developing alternative models [4–6]. In our previous paper [7], using molecular dynamics simulation we found that parts of our silica glass model undergo large tetrahedral

‖ Author to whom any correspondence should be addressed.

0953-8984/00/378041+24$30.00

rearrangements with little energy cost. We identified those rearrangements as motion in double-well potentials responsible for the two-level tunnelling states of [2, 3]. We observed up to two jumps between the potential minima during the observation period, typically around 30 ps, and found that on average about 30 tetrahedra are involved in each jump event. The model of silica glass that was used was relatively small and contained 216 SiO_4 units. In this paper we simulate larger structures with different topologies and containing 512 or 4096 SiO_4 tetrahedra. We find that the larger structures become increasingly floppy in terms of being able to sustain large-amplitude tetrahedral rearrangements. In larger structures, jump events involve groups of atoms in various parts of the structure and which, unlike in smaller structures considered previously in [7], participate in jump events independently of each other. The jump events become more frequent and involve in total more participating atoms. Tetrahedral rearrangements, thus being well represented, may prove to be important in the overall low-energy dynamics of silica glass. This can make it possible to estimate the effect of the presence of two-level tunnelling states on the system's anomalous thermal properties [1] using a technique which incorporates quantum effects of tunnelling.

In addition to addressing the issue of the presence of double-well potentials and two-level tunnelling states in silica glass, we also study the ability of silica glass to support low-ω 'floppy modes' [8, 9] and the similarity of silica glass and β-cristobalite in terms of being able to support those modes. We have recently shown by means of inelastic neutron scattering that the vibrational density of states of silica glass is remarkably similar to that of α-cristobalite, particularly in relation to the so-called 'boson' peak at around 5 meV [10]. This suggests that the atomic motions associated with the boson peak are similar in the two cases; we showed for α-cristobalite that they are related to the acoustic modes with wave vectors approaching the Brillouin zone boundary, where $\partial\omega/\partial k \sim 0$. This picture is consistent with that deduced from other inelastic neutron scattering measurements [11], and recent simulation work [12].

In our previous paper [7] we studied floppy modes in silica glass by applying our 'rigid-unit-mode' model [13, 14]. This model was developed earlier to study floppy modes in crystalline networks of corner-linked polyhedra such as SiO_4 tetrahedra, including the crystalline phases of silica [13, 15–17]. The rigid unit modes (RUMs) are normal-mode vibrations that can propagate without the polyhedra distorting, and are the modes of lowest energy. Formally these are equivalent to the floppy modes discussed for other network glasses. We found that silica glass and β-cristobalite are strikingly similar in their ability to support RUMs. The model of silica glass used in [7] to find and analyse the RUMs contained 216 SiO_4 tetrahedra. In this paper we develop this earlier study using structures with different topologies, each containing larger numbers of atoms. We find here that larger structures of silica glass still show the same degree of RUM flexibility as β-cristobalite. The similarity in the way that silica glass and β-cristobalite are able to support RUMs/floppy modes also follows from the comparison of the low-ω ranges of calculated vibrational densities of states for those structures. We relate this similarity to the structural similarity between silica glass and the corresponding high-temperature crystalline phases which had been previously pointed out in [18–20]. We have argued elsewhere that this structural similarity can be understood from the fact that silica glass is able to use the same RUM flexibility of its crystalline phases in order to allow for random connectivity within the constraints imposed by the formation of an infinite network [14, 19, 20].

2. Generation of silica glass configurations

Silica glass, one of the principal network glass-forming systems, is well described as the continuous random network of vertex-connected SiO_4 tetrahedra. Justification for this comes

from diffraction studies [21], reverse Monte Carlo [22] and molecular dynamics simulations [23], and model building [24, 25]. For simulation work it is necessary to have samples that reflect the random network, but with periodic boundaries to avoid problems associated with surfaces. The use of periodic boundary conditions imposes tight constraints on the formation of the network, and many algorithms suffer from difficulties in producing models that are completely free of defects.

Our approach to generating models of silica glass for this work is to start with defect-free models of amorphous silicon which have periodic boundary conditions. These structures were generated by randomizing the ideal diamond structure and further relaxing it to the lowest metastable state to get the configuration whose correlation functions fit the experimental data. The details of this method are described in [26,27], and the configurations were kindly provided by Professor M Thorpe. Some of the configurations contained four-membered rings of atoms, and others were free of these rings. To convert these configurations to silica we inserted oxygen atoms in the middle of each pair of silicon atoms, to create a network of vertex-connected SiO_4 tetrahedra.

Our prototype silica glass structures were then relaxed using the molecular dynamics simulation method, in particular to allow the linear Si–O–Si bonds to relax to the usual bent

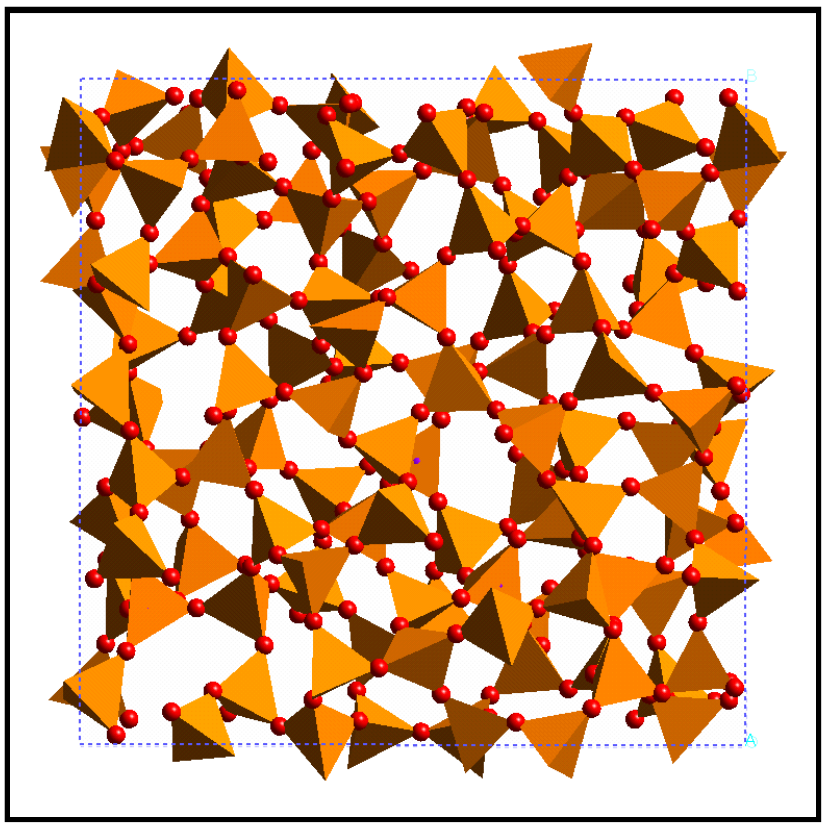

Figure 1. The atomic structure of one of the silica glass configurations used in this study, obtained from an initial configuration of silicon by placing an oxygen atom between each pair of neighbouring silicon atoms, and then relaxing the structure by molecular dynamics simulation.

(This figure is in colour only in the electronic version, see `www.iop.org`)

state. From diffraction measurements on amorphous and crystalline silicates it is known that the mean value of the Si–O–Si bond angle is close to 145°. In the molecular dynamics simulations, both to relax the structure and then to perform subsequent analysis calculations, we used the Tsuneyuki interatomic potential [28] derived from *ab initio* Hartree–Fock self-consistent-field calculations for small clusters of silica. The simulations were performed using the DLPOLY molecular dynamics code [29], and for the basic relaxation of the structure the simulations were performed using a constant-temperature algorithm with the temperature set at 50 K. Using this procedure, we derived a number of silica glass structures with different topologies, with and without four-membered rings of tetrahedra, and containing 216, 512, and 4096 SiO_4 tetrahedra each. An example of one of the relaxed glass configurations is shown in figure 1.

In order to validate the structures that we have produced, we calculated the partial radial distribution functions $t(r) = 4\pi r g(r) = n(r)/r$ for each of our configurations, and compared them with experimental partial functions obtained by reverse Monte Carlo modelling of silica glass [22]. One comparison is given in figure 2, and the comparisons for different configurations look similar. The Si–O and O–O peaks are sharper in the simulation because of the temperature being lower (50 K) than in the experiment (300 K). The Si–O peak in the simulation is also at a slightly larger distance than in the experiment, which is a feature of the interatomic potential. The Fourier transform of the radial distribution function results in the structure factor function $Qi(Q)$ [21]. This is compared with experimental results [21] in figure 3. The comparison shows the very good quality of the derived structures. The main differences between the experimental data and simulation results reflect the differences seen in the $t(r)$ functions: the cooler temperature resulting in sharper $t(r)$ peaks is reflected in the greater amplitude of the oscillations in $Qi(Q)$ at higher values of Q. The slightly larger Si–O distance in the simulation

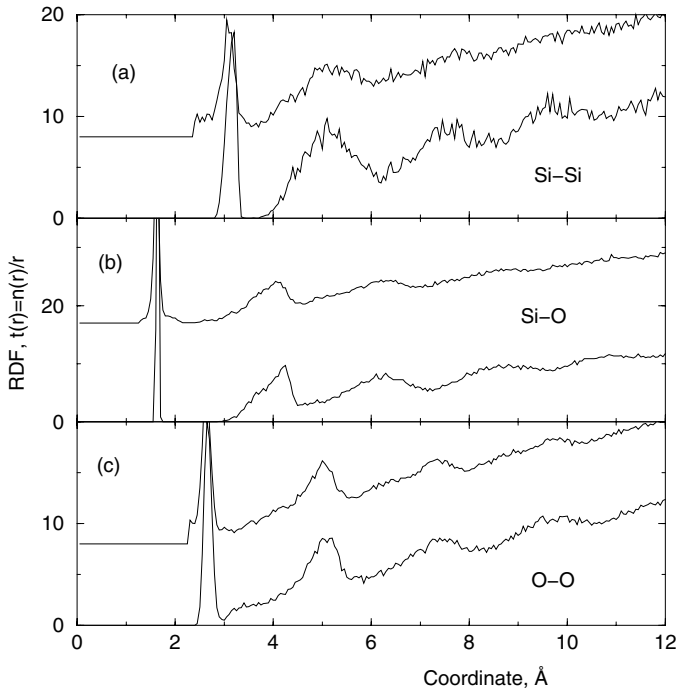

Figure 2. Partial radial distribution functions $t(r)$ of the generated structure of silica glass (lower plots) and experimental data [22] (upper plots) for Si–Si (a), Si–O (b), and O–O (c).

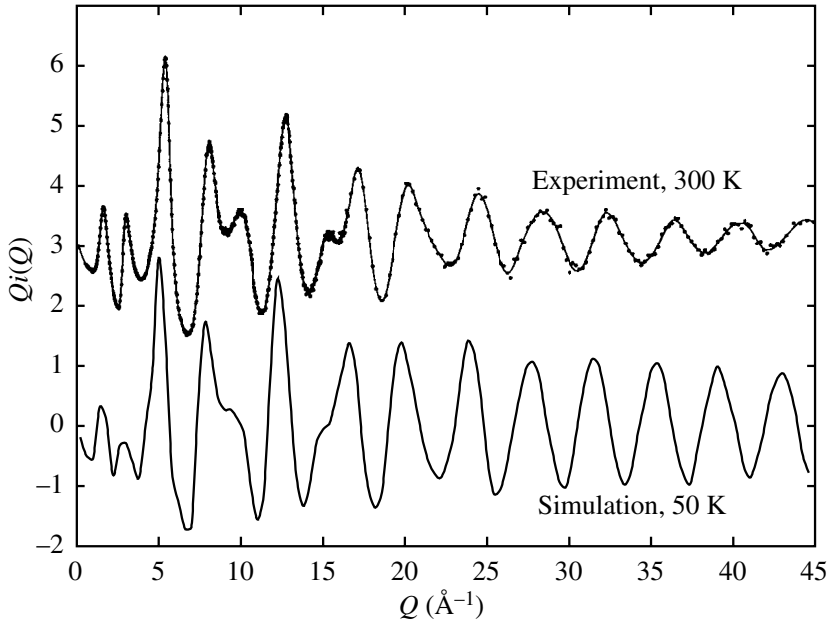

Figure 3. The structure factor $Qi(Q)$ calculated from one of our configurations of silica glass (upper plot) compared with experimental data [21] (lower plot).

leads to the oscillations in $Qi(Q)$ at higher values of Q having a slightly lower period in Q. These discrepancies aside, the agreement between the simulation and experimental $t(r)$ and $Qi(q)$ functions is very good.

3. Two-level tunnelling states in silica glass

3.1. Tetrahedral rearrangements

We start by demonstrating that our silica glass structures contain regions which experience the effect of the presence of double-well potentials. In order to observe a characteristic motion in the double-well potentials it is first necessary to identify those atoms which may participate in such a motion. It was proposed in [2, 3] that atomic motions in double-well potentials in silica glass involve rigid rotations or displacements of SiO_4 tetrahedra. We naturally assumed that the corresponding displacements of atoms in these types of motion significantly exceed those caused by the thermal vibrations around equilibrium positions at low temperature. To select those atoms which may participate in motion in double-well potentials, we constructed the distribution of average square displacements of all atoms. Using the data from molecular dynamics simulation production runs at low temperature, we calculated $\sigma = \langle |\boldsymbol{r}|^2 \rangle - |\langle \boldsymbol{r} \rangle|^2$ for each atom, where $\boldsymbol{r}$ is the position of the atom within the sample, and formed the probability distribution function $P(\sigma)$. An example of $P(\sigma)$ is shown in figure 4. By noting the larger values of σ it is possible to identify the atoms that could possibly participate in large jumps between two minima of double-well potentials. The larger values of σ in figure 4 (values up to 0.2 Å^2) were analysed in terms of which atoms were involved, and it was found that around $2/3$ were oxygen atoms. This is consistent with the involvement of whole-tetrahedral motions, and is consistent with the data derived in [30]. Note that in constructing $P(\sigma)$ we used the

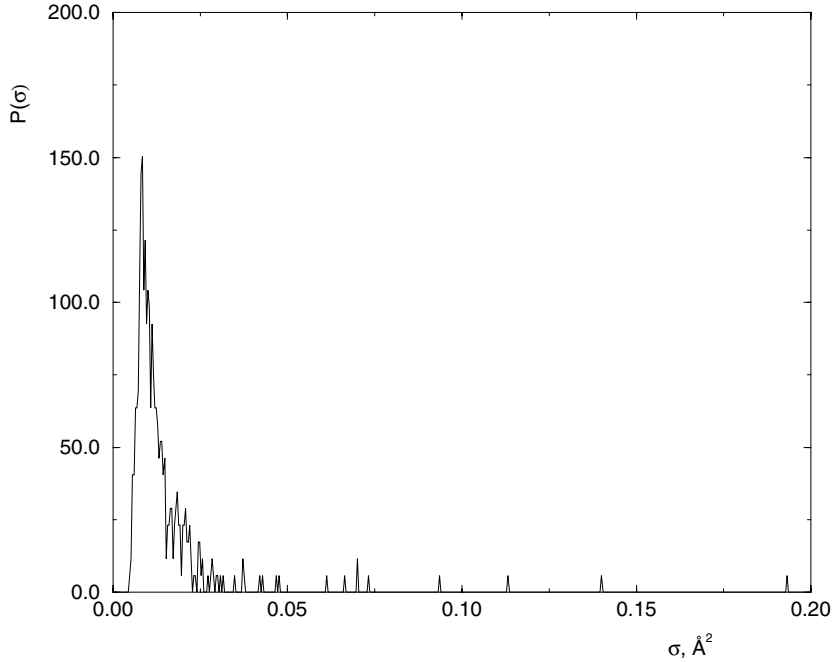

Figure 4. The distribution of atomic average square displacements $P(\sigma)$.

set of σ-values calculated for equal time periods before and after the jump, so $P(\sigma)$ reaches maximum values and is made as sensitive as possible to small jumps.

For the atoms with the largest values of σ from two different simulations we show the time dependence of their coordinates x, y, z in figure 5. The event seen in figure 5(a) involves the atom jumping between from one metastable position to another, and then subsequently jumping back to the original position. Similar changes in coordinates are found for other atoms involved in this event with large values of σ. On the other hand, the event shown in figure 5(b) from a different simulation run has the atom jumping from one position to another but without the atom subsequently returning to its original position. The largest value of the atomic displacements in the observed events is typically around 0.8 Å, which is slightly larger than that found in [30]. Events which involve more frequent jumps between equilibrium positions can be observed in the simulation runs for the structures of larger size, a point to which we return later.

From our analysis of the structure before and after the jump we conclude that this jump results in rotations and displacements of connected tetrahedra, with a few atoms having large displacements in the centre of the cluster of atoms that move, and with the displacements becoming smaller for atoms further away from this centre. Fragments of the structure which experienced the tetrahedral rearrangements associated with the events of figure 5(a) and figure 5(b) are shown in figure 6(a) and figure 6(b), where the initial configuration and the configuration after the jump are superimposed in order to highlight the scale of the jump motions. For jump motions we have calculated the participation ratio, defined as

$$\mathcal{P}_{\text{jump}} = \left(\sum |\boldsymbol{u}_{\text{jump}}|^2\right)^2 \Big/ \left(N \sum |\boldsymbol{u}_{\text{jump}}|^4\right) \tag{1}$$

where $\boldsymbol{u}_{\text{jump}} = \boldsymbol{r}_{\text{after}} - \boldsymbol{r}_{\text{before}}$ is the difference between the coordinates after and before the

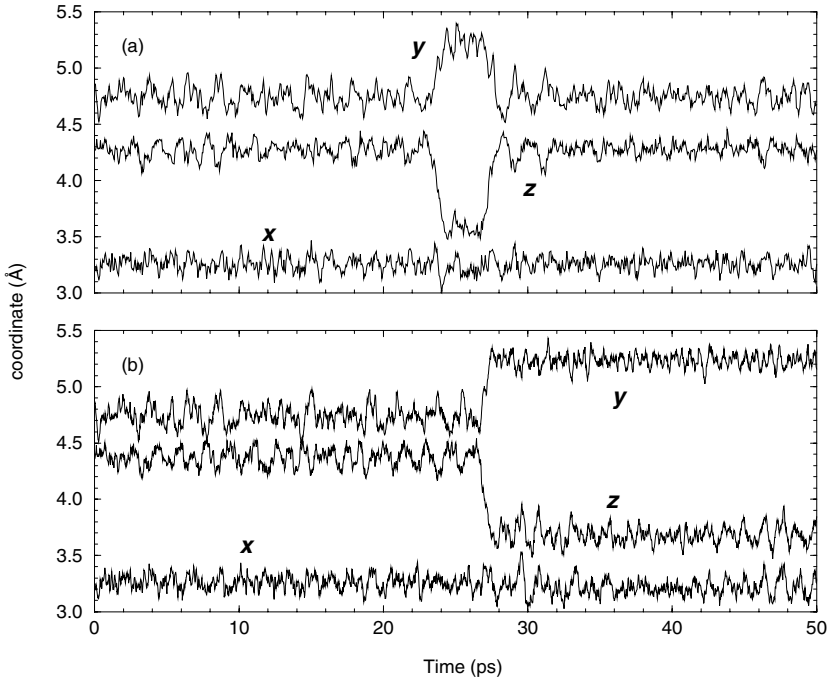

Figure 5. Time dependences of the atomic coordinates x, y, z (in orthogonal Å units) showing an atom undergoing a large jump involving a movement of about 0.8 Å and subsequent jump back (a) and an atom in a different simulation run which oscillates around the new equilibrium after the jump (b).

jump. For a collective motion in which all atoms participate equally, $\mathcal{P}_{\rm jump} \sim 1$, whereas for a motion involving a single atom, $\mathcal{P}_{\rm jump} \sim 1/N$. The value of $\mathcal{P}_{\rm jump}$ for the event shown in figure 5(b) gives the number of tetrahedra participating in this event, equal to a value of $N\mathcal{P}_{\rm jump}$ of around 30. This is consistent with the number deduced from $P(\sigma)$ by counting the number of σ-values greater than a lower threshold, which was set as the upper edge of the large peak in $P(\sigma)$ in figure 4: this lower threshold is assumed to set the upper limit given by simple thermal vibrational motion without jumps. We have found similar participation numbers for other jump events that we have analysed.

Animations of the jump events, showing whole-tetrahedra reorientations, were made from the molecular dynamics simulations and are available in the electronic version of the journal. They can also be viewed from http://www.esc.cam.ac.uk/movies.

There is an alternative way to explore the ability of our structure to undergo large-amplitude reorientational motions. The structures used for production runs in the molecular dynamics simulation were generated from the initial configurations by relaxing the initial configurations, which by design had linear Si–O–Si bonds. In all cases the final configurations had Si–O–Si bond angles distributed around 145°. We produced different initial relaxed configurations by using different sets of initial atomic velocities in the molecular dynamics simulations. If there is large-amplitude flexibility in the structure, this should enable different relaxations to produce configurations that correspond to different minima of the free energy that are related to the configurations produced by the large-scale jump motions that we have just been discussing.

We have compared different resulting structures by taking the differences between the coordinates of the same atoms in different relaxations, $\boldsymbol{u}_{1,2} = \boldsymbol{r}_1 - \boldsymbol{r}_2$, and using these to

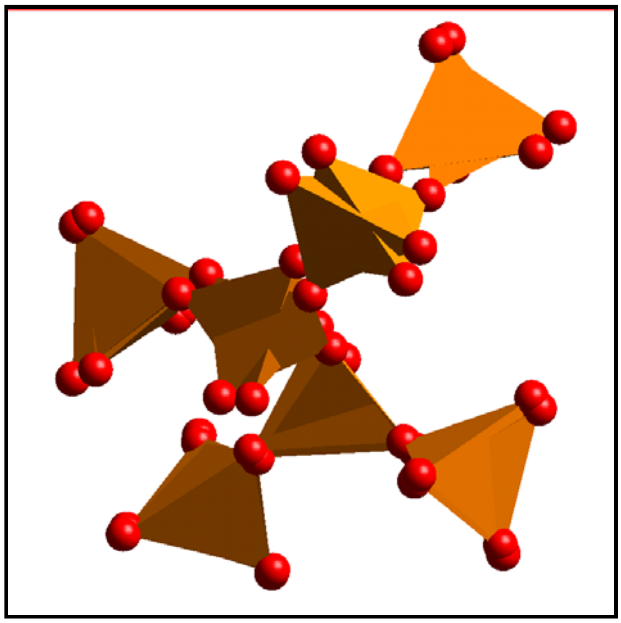

(a)

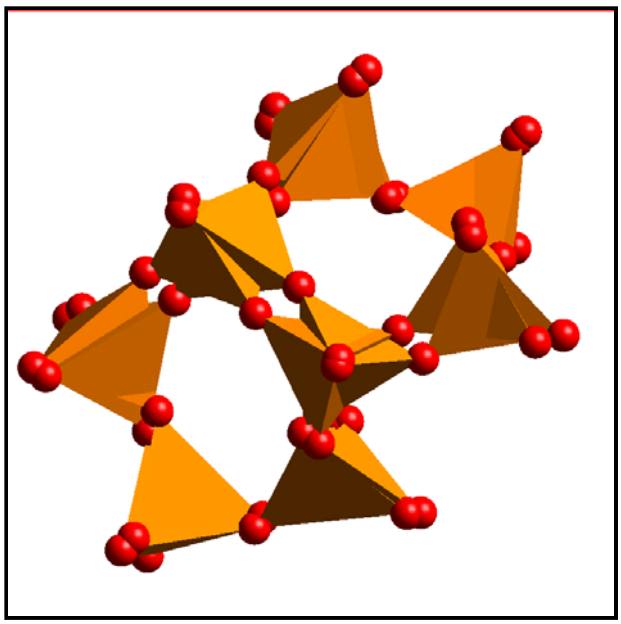

(b)

Figure 6. Snapshot images of the tetrahedra participating in the jump events indicated in figure 5. The figure shows superimposed snapshots of the local configuration captured before and after the jump event in order to highlight the large-amplitude reorientational motions. Animations of the jump events, showing whole-tetrahedra reorientations, are available in the electronic version of the journal (animations are in mpeg format and are of 2.2 and 2.9 Mbyte size). They can also be viewed from http://www.esc.cam.ac.uk/movies.

(This figure is in colour only in the electronic version, see `www.iop.org`)

calculate the corresponding participation ratio:

$$\mathcal{P}_{1,2} = \left(\sum |\boldsymbol{u}_{1,2}|^2\right)^2 \Big/ \left(N \sum |\boldsymbol{u}_{1,2}|^4\right). \tag{2}$$

The value of $\mathcal{P}_{1,2}$ for the differences between two relaxed configurations shows that the changes involve around 100 tetrahedra. Analysis of the atoms involved shows that in each case it is a subset of this group of tetrahedra that is involved in the large-amplitude jump displacements described above. This clearly suggests that our network contains regions that are floppy in terms of their ability to support large-amplitude reorientational motions within a more rigid framework.

3.2. The potential energy barrier

We suggest that the motions of the type that we observe in figure 5 and figure 6 occur in the double-well potentials that give rise to two-level tunnelling states [2, 3]. It is interesting to determine the values of the energy barrier separating two potential minima and the energy difference between minima. We plot in figure 7 the potential energy of the whole system in the constant-total-energy simulation. During this time period part of the structure undergoes a jump from one equilibrium position to another. No change in energy can be seen at the moment of the jump, according to figure 7. Any possible change is clearly substantially lower than the thermal fluctuations. In order to determine values of the energy barrier and difference between minima, we have relaxed the structures either side of the jump event and half-way through the jump event (i.e. the transition state) using the molecular dynamics code at 0 K. For the configuration in the transition state we pinned the position of the atom that moves the most in order to prevent the state from relaxing to either of the states either side of the transition state.

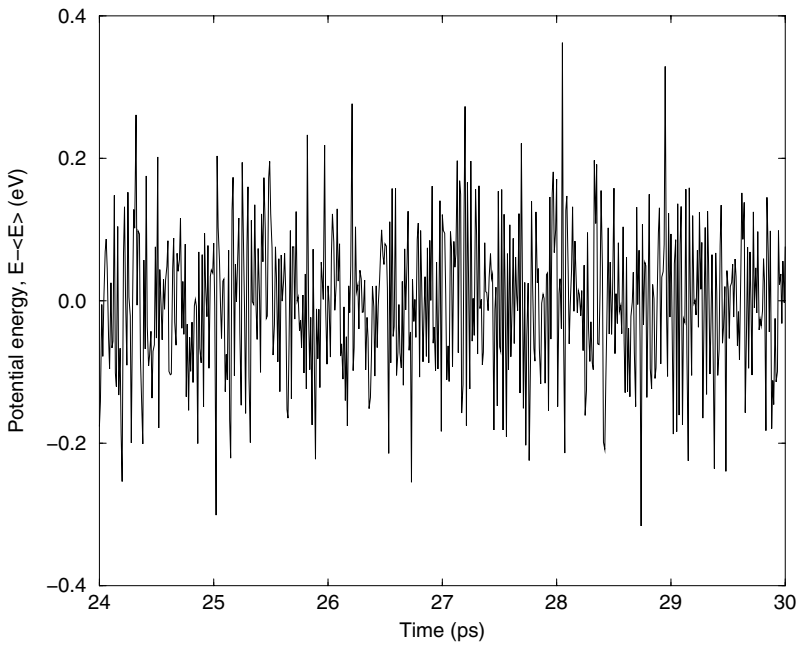

Figure 7. The time dependence of the potential energy of the simulation sample (with its average value subtracted) through the jump event shown in figure 5(b) and figure 6.

This procedure gave an energy barrier of 0.06 ± 0.02 eV (for about 30 tetrahedra; see above), and the energy difference between the potential minima is less than 0.01 eV. The uncertainties arise from numerical errors in the simulations that are hard to control to greater precision because of their small size relative to the total system energy. Our estimates of the size of the energy barrier and the energy difference are within the ranges proposed by [2, 3].

Having estimated the parameters of the double-well potentials, we address an interesting point about the dynamics of motion of our structure in the double-well potential. It is evident that the system can remain in one potential minimum for times corresponding to many periods of oscillation of SiO_4 tetrahedra before jumping to another state (figure 5), which implies that the energy barrier separating two minima is much larger than the thermal energy fluctuations. However, we do not see any change in potential energy through the jump in figure 7. As the system evolves through the cooperative small-amplitude oscillations of the tetrahedra, it finds the path in the phase space with the energy barrier small enough (around 0.06 eV in our measurement) to allow it to jump into another potential minimum with little energy cost and thus to avoid crossing a barrier separating equilibrium states which would be inaccessibly high otherwise. Of course, for quantum tunnelling it will be possible for jump events to sample more of the energy barriers than the one determined by this path in phase space.

3.3. Simulating larger structures

We note that in smaller structures with 216 SiO_4 tetrahedra we generally observe two spatially distinct regions in the structure where groups of tetrahedra experience simultaneous large-amplitude reorientations, or two 'active' regions. In order to preserve the connectivity of the structure, the surrounding of the region which experiences large tetrahedral reorientation distorts as well, with deviations diminishing with the distance from that region. Since the distance between two 'active' regions is only several tetrahedra, any large reorientation of tetrahedra in one 'active' region depends on the reorientation in another. To illustrate the interaction between 'active' regions, let P_1 be the point in the phase space defined by the coordinates and velocities of the tetrahedra in the first 'active' region, t_1 is the moment of time when P_1 favours the jump across the potential energy barrier in that region, and P_2, t_2 are the corresponding phase-space point and time for the tetrahedra in the second 'active' region. If at t_1 atoms in the first region approach P_1 and atoms in the second region are not far from P_2, then a jump of atoms in the first region may trigger a jump of atoms in the second, and vice versa. However, if at t_1 the atoms in the second region are far away from P_2, the jump in the first region will not happen because the connectivity of the network precludes large-amplitude rotating of one group of tetrahedra without distorting the tetrahedra in the adjacent region. In this picture, tetrahedral rearrangements happen simultaneously and only at times when atoms in the first and second 'active' regions reach P_1 and P_2, correspondingly. In fact, to make the jump possible in two regions simultaneously, both P_1 and P_2 should favour the jump over the largest of two barriers in each region. In this picture, 'correlated' jump events may be observable much less often than if the interaction between 'active' regions is reduced or absent. In the structure with 216 SiO_4 tetrahedra we observed only up to two jump events during an observation period of 30 ps.

The picture becomes different when we simulate larger structures containing 512 and 4096 tetrahedra. Together with an increased number of atoms participating in large jumps, we observe that the frequency of large jumps increases considerably—we see up to ten jump events in the simulation runs of the structure with 512 tetrahedra during the same simulation period and even more for larger structures. In larger structures, tetrahedral rearrangements which happen in different 'active' regions are much less correlated with each other than they are in smaller

structures, and occur much more frequently. This means that silica glass structures, if selected to be large enough, are considerably floppy in terms of being able to support large-amplitude tetrahedral rearrangements. In other words, if the structure is chosen to be large enough, the potential barrier which needs to be overcome by a group of tetrahedra is effectively reduced. If quantum effects are incorporated into simulation, the reduced potential energy barrier can enable tunnelling between minima to occur more often.

The increased possibility for tunnelling due to the effective reduction of the potential energy barrier and the total increase of the number of atoms participating in jump events in larger structures mean that this type of motion can make a significant contribution to the low-energy dynamics of the system. It therefore may be possible to estimate the effects of the presence of two-level tunnelling states on the thermal properties of the system, if quantum effects are incorporated into the simulation. This can be done in the path integral molecular dynamics simulation technique. The development of this technique for the application to systems like silica glass is currently being carried out.

It should be noted that attempts to find double-well potentials were made previously for metallic and other glasses. Earlier attempts were based on the assumption that it is the single atom that moves in the double-well potential [31, 32]. Later works [33, 34] assumed that the objects moving in double-well potentials are groups of atoms. The common approach to finding and studying double-well potentials in glasses involves making assumptions regarding the size of objects moving in the double-well potential (being either individual atoms or groups of atoms of a certain size) and then searching for the alternative potential energy minimum by spatial rearrangement of those objects. Using a similar approach, a search for double-well potentials in silica glass in particular was carried out in [30]. In more recent papers [35, 36] the metallic glass was investigated by means of a molecular dynamics simulation run with a certain low-temperature localized vibrational mode assumed to describe atomic motions in a double-well potential, forcibly launched at the start of simulation. In our method of finding and studying double-well potentials in silica glass, we do not make any initial assumptions regarding their nature, including the location, size, dynamics, and other spatial or dynamical features; neither do we initially stimulate the system. We have used a simpler and in a way more natural approach, letting our glass system freely evolve in the molecular dynamics run and explore its trajectories in the phase space.

4. Floppy modes in silica glass

4.1. Floppiness of the amorphous silica structure: Maxwell counting

In studying the low-energy vibrational modes of silica glass, it is assumed that any low-energy distortion of a silicate structure will have a minimal deformation of the constituent SiO_4 tetrahedra [37, 38], since these units are fairly stiff and any significant deformation will be accompanied by high-frequency modes. Whether an infinite framework of corner-linked SiO_4 tetrahedra can vibrate without the tetrahedra distorting is actually a very subtle issue. As noted above, the vibrational modes that do not involve distortions of the interatomic bonds are usually referred as 'floppy modes' in the context of network glasses [8, 9] or rigid unit modes in the context of crystalline framework structures [13, 15–17]. In a model in which the only forces are those associated with stretching of bonds or distortions of polyhedra, the RUMs/floppy modes will have identically zero frequency [15].

The usual approach to analysing the flexibility of a structure is to use the procedure of 'Maxwell counting' [39]. In an atomic system, such as the chalcogenide glasses, it is taken that each atom has three degrees of freedom, and each bond gives one constraint to the system.

The number of RUMs/floppy modes is equal to the difference between the number of degrees of freedom and the number of constraints [8,9]. In a system such as silica, where there are rigid SiO_4 tetrahedra and separate Si–O and O–O bonds, this procedure will lead to an overcounting of the number of constraints, since the rigidity of a SiO_4 tetrahedron is ensured by only nine of the ten bonds. We tend to prefer an alternative way of counting degrees of freedom, which is to associate six degrees of freedom with the rigid-body motions of a tetrahedron, and to associate three constraints with every bridging oxygen (that is, every oxygen that is part of two tetrahedra) [15, 17]. The two methods of applying the Maxwell counting procedure give identical results. The Maxwell counting procedure gives an interesting result when applied to silica. For a network of vertex-connected tetrahedra, the total number of degrees of freedom equals the total number of constraints, so the structure of silica, either amorphous or crystalline, is neither floppy nor overconstrained, but balanced between the two extremes. Thus one cannot easily predict whether the floppy modes envisaged in [37, 38] can exist in silica glass.

We have recently developed this approach in detailed application of the RUM model to framework crystalline structures of silicates, originally in an attempt to determine the ways in which the crystal structure of a framework silicate can distort in order to allow a displacive phase transition to occur [13, 15–17]. The RUM approach has turned out to be of more general use than the initial search for mechanisms of displacive phase transitions, and has encompassed phenomena such as negative thermal expansion [40–42] and zeolite activity [43, 44], as well as providing more detailed quantitative insights into the thermodynamic properties of phase transitions [45].

A major component of our RUM model has been the development of an effective tool to facilitate the identification of RUMs/floppy modes in framework silicates. Noting that a RUM is a phonon normal mode that can propagate without requiring the distortions of the SiO_4 tetrahedra, the task is to set up the dynamical matrix in such a way that RUMs are obtained as zero-frequency solutions. Our approach is to treat the SiO_4 tetrahedra as rigid units within the framework of molecular lattice dynamics, and to replace all the bridging oxygens by pairs of atoms that are associated with one tetrahedron or the other. The pairs of split atoms are held together by harmonic spring forces of zero equilibrium length, which act to resist any motion that moves them apart. This is illustrated in figure 8. The 'split-atom' method [15, 17] has been implemented within the formalism of harmonic molecular lattice dynamics, using a program called CRUSH [46].

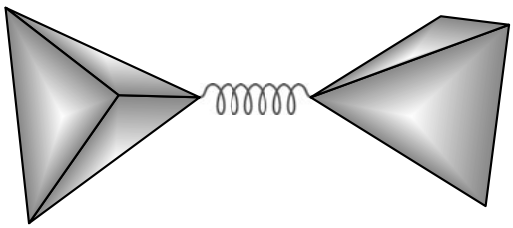

Figure 8. Representation of the split-atom method [15]. The spring has an equilibrium length of zero, and a force constant set to a value that best mimics the stiffness of the SiO_4 tetrahedra as judged from measurements of phonon frequencies.

In the application of the RUM split-atom model to various crystalline forms of silica it was found that symmetry can cause some of the constraints to be degenerate, resulting in a non-zero number of zero-frequency RUMs. The number of RUMs, as well as the values of the wave vectors $\boldsymbol{k}$ at which these RUMS exist, were found to be different for crystalline forms of different symmetries [13, 16, 17]. This is the breaking of the strict Maxwell criterion discussed

above. The question that we now address is that of whether there are RUMs in silica glass, noting in advance the caveat that there is no symmetry corresponding to that found in the crystalline phases.

4.2. Rigid unit modes in silica glass

In crystalline silicates, it was often found that the RUMs lie on special planes of wave vectors, determined by the symmetry [13, 17]. There are no corresponding sheets of wave vectors in silica glass, so the same type of search method will not be appropriate. Instead we use a density-of-states search method for the determination of the RUM flexibility of silica glass [17,47]. In essence, we solve the dynamical matrix within the CRUSH split-atom method for a random set of wave vectors and form the density of states $g(\omega)$. Random wave vectors are used because a grid imposed on a symmetric structure was found to produce periodic structure in the resultant density of states. The CRUSH density-of-states search method gives the usual Debye result, $g(\omega) \propto \omega^2$ as $\omega \to 0$, when there are no RUMs, and $g(\omega) \sim$ constant as $\omega \to 0$ when there are RUMs [47]. It should be noted that the $g(\omega)$ produced this way is not to be confused with the $g(\omega)$ of a real material, because in a real material the full set of force constants would give non-zero values of the RUM frequencies and so we would not get $g(\omega \to 0) \sim$ constant. Instead, the CRUSH $g(\omega)$ should be seen as a particular diagnostic tool with the purpose of giving a unique quantitative assessment of the RUM flexibility of a framework structure, and to make this distinction clear we will use the special designation of $g_C(\omega)$ for the RUM/CRUSH $g(\omega)$.

We have calculated $g_C(\omega)$ for our silica glass configurations, and the results are given in figure 9. There the $g_C(\omega)$ for silica glass is compared with $g_C(\omega)$ of β-cristobalite. The

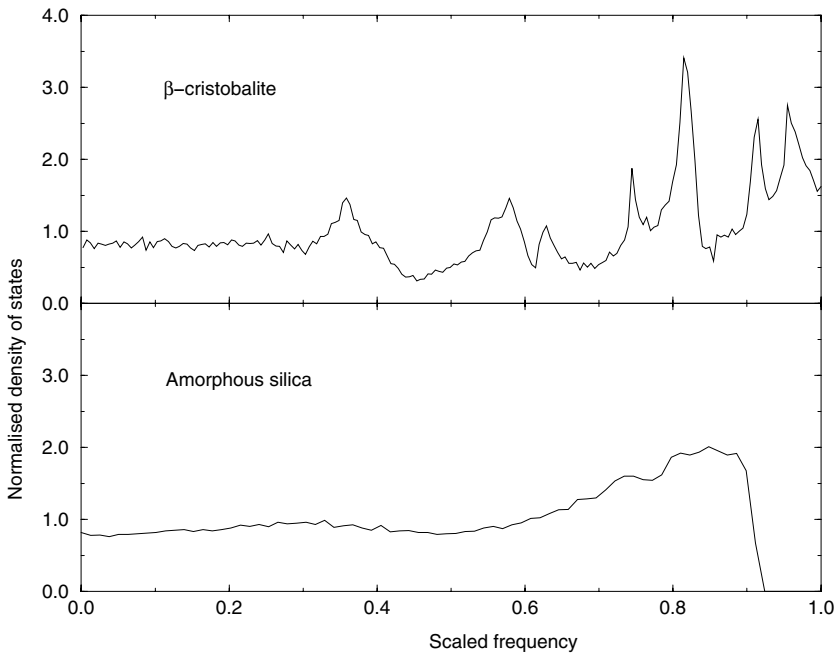

Figure 9. The density of states, $g_C(\omega)$, calculated using our split-atom method, for β-cristobalite and silica glass. The values of the frequencies are determined by the spring force constant in the split-atom method, and have been scaled against the maximum frequency in this figure.

similarity of the $g_C(\omega)$ for the two systems for $\omega \to 0$ is striking—in fact, one can view the overall form of $g_C(\omega)$ of silica glass simply as a lower-resolution version of $g_C(\omega)$ of β-cristobalite. This comparison implies that silica glass has the same RUM flexibility as β-cristobalite, which is actually an astonishing result given that the RUM flexibility of β-cristobalite had previously been interpreted as being due to the effects of the high symmetry of its crystal structure [13, 15, 48].

In order to establish the spatial extent of the RUMs in silica glass, we have calculated the participation ratio $\mathcal{P}_C$ using the CRUSH eigenvectors instead of the differences in atomic coordinates as before:

$$\mathcal{P}_C = \left(\sum |\boldsymbol{u}_C|^2\right)^2 \Big/ \left(N \sum |\boldsymbol{u}_C|^4\right) \tag{3}$$

where the $\boldsymbol{u}_C$ are the atomic displacements associated with the CRUSH eigenvectors. If the value of $\mathcal{P}_C$ is close to $\sim$1 for a particular vibration, all atoms participate equally in that vibration. The participation ratio corresponding to the $g_C(\omega)$ of figure 9, bottom panel, is shown in figure 10. As can be seen from figure 10, $\mathcal{P}_C \sim 0.8$ for all ω, including the low-ω modes. This means that the low-ω RUM-like vibrations involve all tetrahedra in the glass, and are not localized to particularly flexible segments of the glass structure.

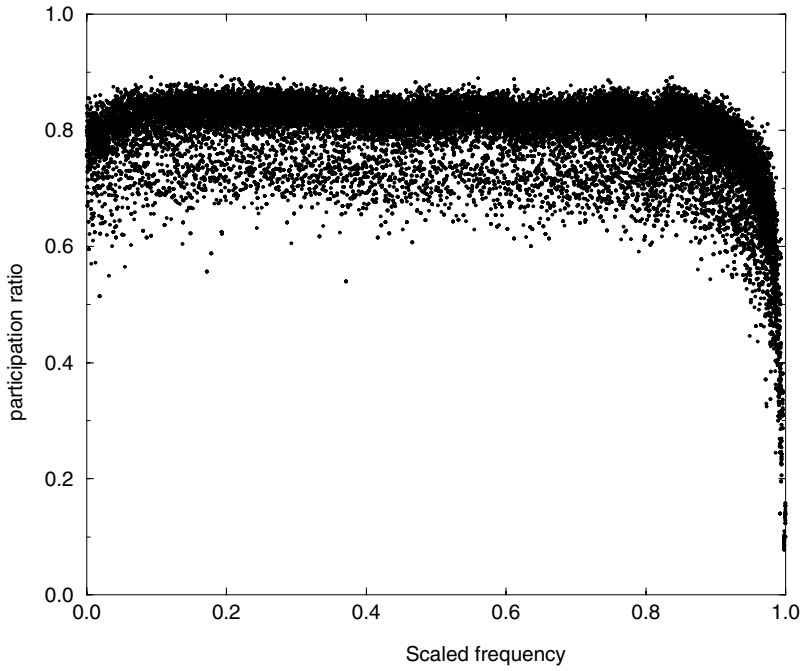

Figure 10. The participation ratio, $\mathcal{P}_C$, calculated using our split-atom method, for all CRUSH eigenmodes from silica glass. The values of the frequencies are determined by the spring force constant in the split-atom method, and have been scaled against the maximum frequency in this figure.

The same RUM flexibility of silica glass and β-cristobalite can give an insight into their structural similarities. As was shown in [18–20], over short length scales there are strong similarities between the structures of amorphous silica and the crystalline tridimite and cristobalite phases of silica. Using reverse Monte Carlo modelling, these similarities were

found to extend over the length scale 0–10 Å [19]. Common RUM flexibility, which includes the flexibility of the rings of connected SiO_4 tetrahedra, gives rise to the possibility for the glass structure to employ structural elements of its high-temperature crystalline phase in producing a disordered yet fully linked network. Thus the structural similarities between the silica glass and its high-temperature crystalline phase may be explained by the inherent RUM flexibility of these structures. This point has been discussed in detail by Keen and Dove [19, 20].

4.3. Inclusion of a Si–Si interaction

We have investigated the effect of introducing an interaction between the nearest-neighbour Si atoms on the low-ω $g_C(\omega)$. This takes the form of a harmonic spring force for each pair of Si atoms defined to have an equilibrium length equal to the actual interatomic distance. This force has the general effect of separating the frequencies of torsional RUM motions, which preserve the size of the Si–O–Si angle, from those of the RUM motions that cause a flexing of the Si–O–Si angle. In some crystalline silicates, this can explain why some RUMs give rise to displacive phase transitions by acting as the classical soft mode, whereas others do not.

The main effect on $g_C(\omega)$ of increasing the size of the Si–Si interaction is shown in figure 11. It can be seen to lead to a reduction and subsequent disappearance of the near-zero-frequency component of $g_C(\omega)$, with a build up of a peak in $g_C(\omega)$ at a slightly higher value of ω. The presence of the Si–Si interaction clearly results in a diminished RUM flexibility of the glass structure.

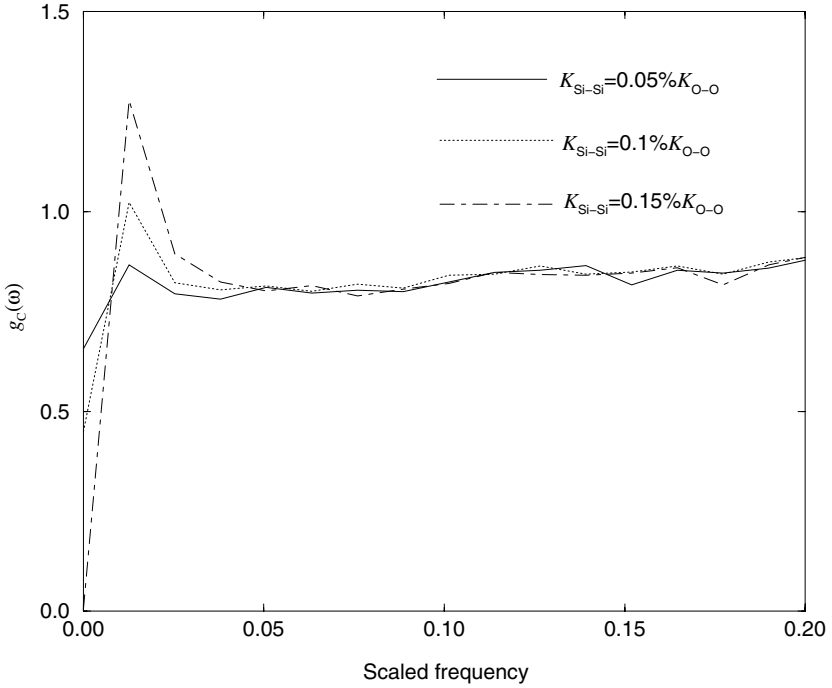

Figure 11. The density of states, $g_C(\omega)$, calculated using our split-atom method, for silica glass with the inclusion of a Si–Si interaction. The different plots show the effect of varying the size of the Si–Si force constant, K_{Si-Si}, expressed as a fraction of the O–O force constant, K_{O-O}. The values of the frequencies are determined by the spring force constant in the split-atom method, and have been scaled against the maximum frequency in this figure.

It should be noted that a comparison of this point with the case for β-cristobalite is not possible since the ideal crystal structure has linear Si–O–Si bonds, and therefore the Si–Si interaction has no effect.

4.4. Inclusion of defects in the silica glass structure

The presence of impurities in silica glass results in the formation of non-bridging Si–O bonds. It is appealing to study what effect this may have on the RUM density of states in our model. We removed some of the SiO_4 tetrahedra, thus creating non-bridging Si–O bonds, and calculated the $g_C(\omega)$ of such a structure, shown in figure 12. The interesting feature is the formation of a peak in $g_C(\omega)$ at $\omega \sim 0$. We note from figure 12 that the new zero-frequency modes come from the low-frequency part of the density of states, which therefore becomes depleted as the number of $\omega \sim 0$ modes increases. This is opposite to the effect of including a Si–Si interaction, but is actually not at all surprising since the incorporation of non-bridging Si–O bonds will lead to a reduction in the number of Maxwell constraints compared to the number of degrees of freedom. The increase in the number of RUMs caused by the incorporation of the non-bridging bonds is consistent with the observation of the increased inelastic neutron scattering intensity found in alkali disilicate glasses over silica glass [10].

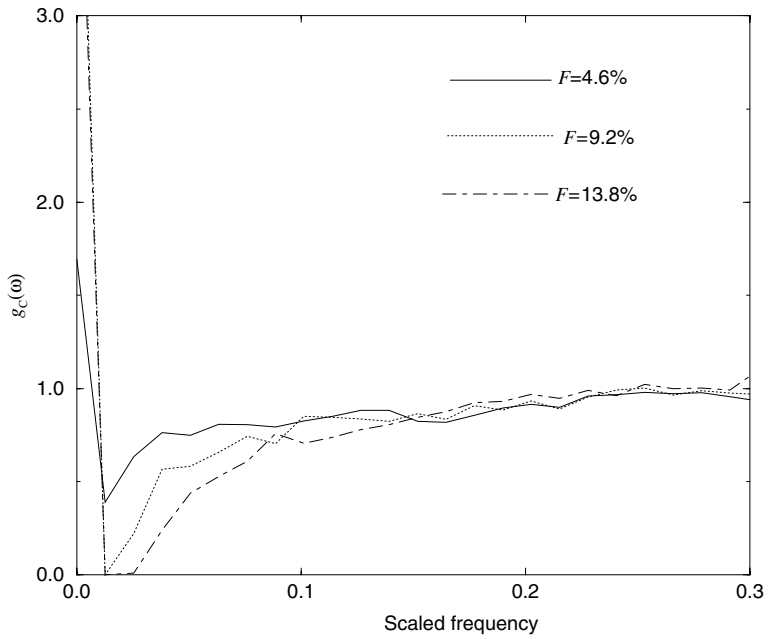

Figure 12. The density of states, $g_C(\omega)$, calculated using our split-atom method, for configurations of silica glass with missing SiO_4 tetrahedra and hence containing non-bridging Si–O bonds. The different plots show the effect of increasing the number of non-bridging bonds as the fraction of missing tetrahedra, F, increases. The values of the frequencies are determined by the spring force constant in the split-atom method, and have been scaled against the maximum frequency in this figure.

The calculated participation ratio of the CRUSH eigenmodes, $\mathcal{P}_C$, for the structure with a fraction of tetrahedra removed is shown in figure 13. The values of $\mathcal{P}_C$ for the new $\omega \sim 0$ modes vary uniformly from 0 to 0.8, showing that some highly localized $\omega \sim 0$ vibrations have appeared, but that the motions of other $\omega \sim 0$ vibrations still involve almost the whole sample.

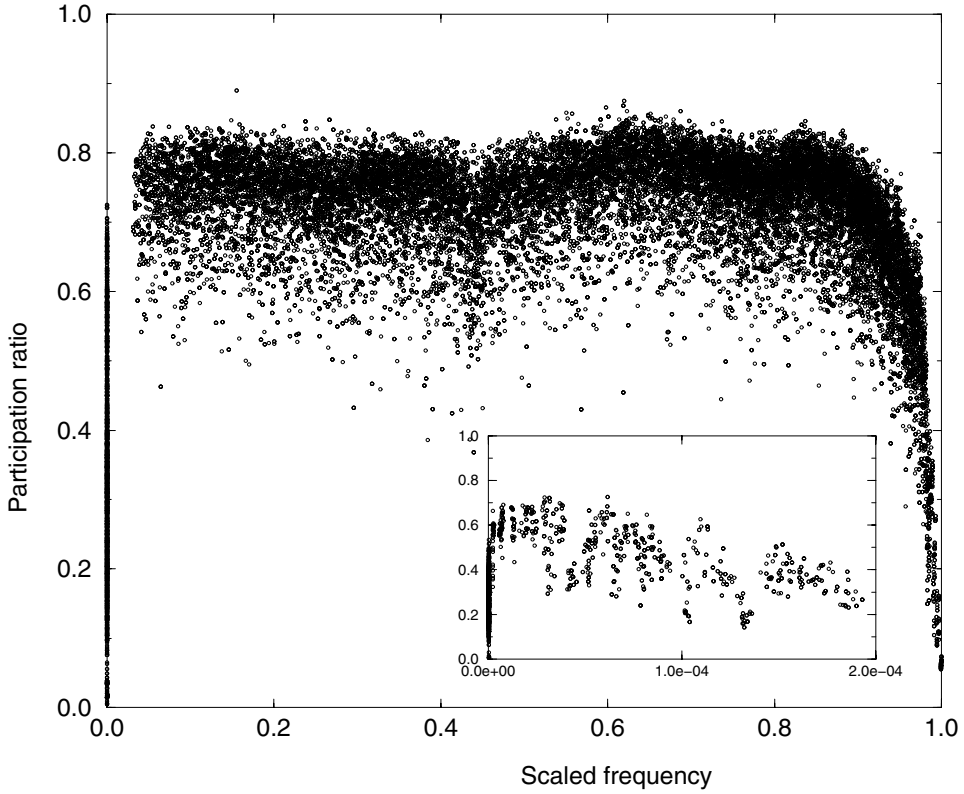

Figure 13. The participation ratio, $\mathcal{P}_C$, calculated using our split-atom method, for all CRUSH eigenmodes from the silica glass configuration with 9.2% of missing SiO_4 tetrahedra. The values of the frequencies are determined by the spring force constant in the split-atom method, and have been scaled against the maximum frequency in this figure.

The spread of values of $\mathcal{P}_C$ for the $\omega \sim 0$ modes is shown as an inset in figure 13. We suggest that this is a pointer to possible behaviour in amorphous silicates that contain non-bridging Si–O bonds, such as K_2SiO_5 [10, 49], and this is being explored in ongoing calculations.

4.5. Size effects

We conclude our discussion of the RUMs in silica glass by noting that in [7] we used only the configuration containing 216 SiO_4 tetrahedra for performing the RUM analysis. We have extended the analysis to larger samples, with up to 4096 tetrahedra, and with or without four-membered rings of tetrahedra. We have found that the same results are valid in all cases, including the conclusions related to the RUM density of states, the spatial extents of RUMs, and other aspects of RUM dynamics.

5. Collective dynamics, and comparison with experimental data

5.1. The vibrational density of states

To further explore the ability of silica glass to support low-frequency floppy modes, we have calculated the vibrational density of states from the molecular dynamics simulations. The

vibrational density of states can be obtained from the single-particle velocity self-correlation function, $C(t)$ [50]:

$$C(t) = \frac{\langle \boldsymbol{v}(0) \cdot \boldsymbol{v}(t) \rangle}{\langle \boldsymbol{v}(0) \cdot \boldsymbol{v}(0) \rangle} \tag{4}$$

where the brackets $\langle \cdots \rangle$ denote an average over time. The one-phonon density of states is the weighted Fourier transform of this correlation function [50].

The velocity correlation function was calculated from the simulations of the sample of silica glass that contained 4096 SiO_4 tetrahedra at different temperatures. The correlation functions were produced over a time range of 6 ps. The calculated Fourier transforms of correlation functions for Si and O atoms were weighted with respective scattering lengths, to arrive at the total vibrational density of states.

We plot the vibrational densities of states of silica glass calculated at two temperatures, 10 K and 300 K, over the frequency range 0–8 THz in figure 14. We note that the behaviour of the density of states in this range does not change significantly as the temperature varies, and calculations for heating up to 1000 K also show little variation in the form of the density of states. In figure 14 we also plot the vibrational densities of states of α- and β-cristobalite obtained from the earlier molecular dynamics simulations of Swainson and Dove [51]. The excess of low-frequency floppy modes in β-cristobalite as compared to α-cristobalite was noted and discussed in [48, 51]. It was shown in [13, 48, 51] that β-cristobalite is able to support more RUMs/floppy modes than α-cristobalite. What can be seen from figure 14 is that in the low-frequency range up to 1.5 THz the density of states of silica glass is closer to that of β-cristobalite than to that of α-cristobalite. This suggests that silica glass is at least as floppy as

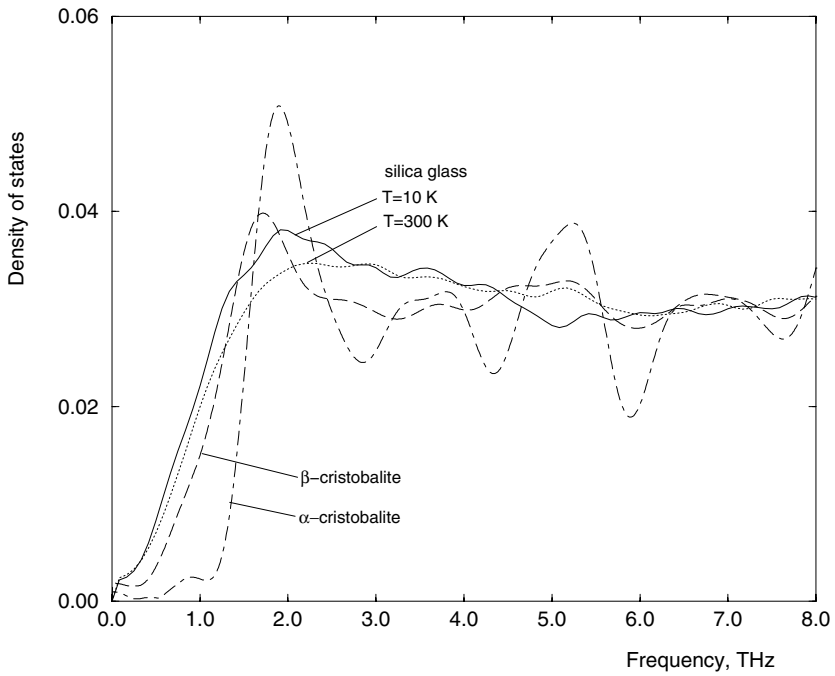

Figure 14. The vibrational density of states, $g(\omega)$, calculated from the molecular dynamics simulation, for silica glass at 10 K (solid line), silica glass at 300 K (dotted line), β-cristobalite (dashed line), and α-cristobalite (dot–dashed line). The cristobalite data are taken from [51].

β-cristobalite as regards being able to support low-frequency floppy modes. This conclusion is consistent with the results of our RUM analysis presented in the previous section.

5.2. Experimental measurement of the dynamic structure factor, S(Q, E)

Previously we have published measurements of the neutron scattering function $S(E) = \int S(Q, E)\ \mathrm{d}E$ for silica glass, polycrystalline α-cristobalite, and amorphous potassium disilicate [49], where Q is the modulus of the scattering vector $\boldsymbol{Q}$ and E is the energy transfer due to absorption or creation of an excitation of energy $\hbar\omega$. The results from this earlier work showed that there are similarities between the inelastic spectra for silica glass and α-cristobalite, but there are indications from the data of an excess density of states at low energy/frequency.

We now report new measurements of the full dynamic structure factor, $S(Q, E)$, of silica glass and α-cristobalite at ambient temperature by means of inelastic neutron scattering. The experiments were performed on the MARI spectrometer at the ISIS pulsed neutron facility. The results of the experiments are maps of $S(Q, E)$ across a range of values of Q between 0 and 8 Å^{-1} and energy transfers E from -10 to 30 meV. The maps are shown in figure 15.

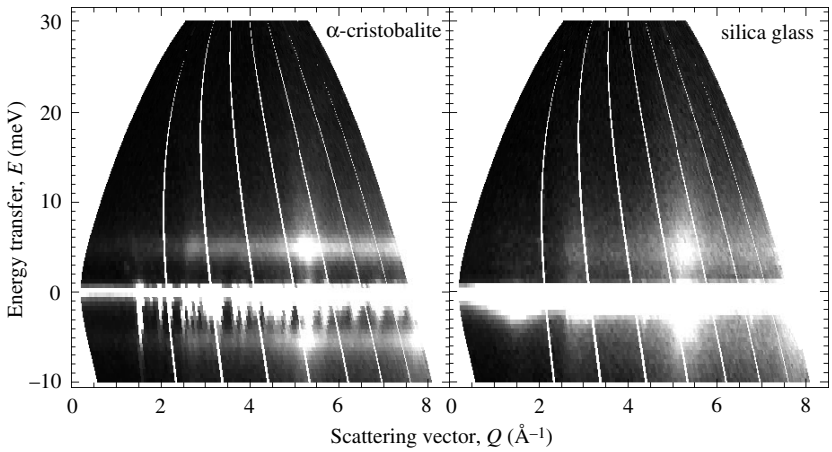

Figure 15. Intensity maps of the inelastic neutron scattering function $S(Q, E)$ for silica glass (right) and polycrystalline α-cristobalite (left), obtained on the MARI spectrometer at ISIS. The larger values of $S(Q, E)$ are indicated by lighter shades of grey in the maps.

The most prominent feature in both maps is the band of inelastic scattering around 5 meV that extends across most of the range of Q. This is the inelastic scattering that is associated with the so-called boson peak, which is seen as the peak at 5 meV in the $S(E)$ data published previously [49]. That the same feature is seen for both polycrystalline and glass phases shows that it is not a particular feature of the glass state—this is a point that will be discussed in more detail elsewhere [52]. The striking similarities between the maps for the two phases are reinforced by noting that the inelastic scattering at 5 meV is enhanced in two regions of Q, between 2.5 and 3 Å^{-1}, and between 5 and 5.5 Å^{-1}.

The main difference between the two maps is that the band of inelastic scattering at 5 meV is more spread out in energy in the glass data, and in particular rather more of the inelastic scattering spreads to lower energy. By comparison of these results with the density-of-states data from the molecular dynamics simulations above, we can identify this spread of inelastic scattering to lower energies as being related to the low-energy excitations studied earlier in this paper, namely the RUMs/floppy modes.

In the following calculations we will aim to interpret the $S(Q, E)$ map for silica glass in terms of some of the insights from the calculations in the previous sections of this paper.

5.3. The dynamic structure factor S(Q, E) from molecular dynamics simulation

We have calculated the dynamic structure factor for silica glass from our molecular dynamics simulations. The main difference between calculations for a crystal and for an isotropic material (such as a non-crystalline material or a polycrystalline material) is that in the latter case the scattering function $S(\boldsymbol{Q}, \omega)$ has to be averaged over all orientations of the scattering vector $\boldsymbol{Q}$. In our formalism we build this orientational average in from the start. The intermediate-scattering function, $F(\boldsymbol{Q}, t)$, is defined as [50]

$$F(\boldsymbol{Q}, t) = \sum_{ij} b_i b_j \left\langle \exp(\mathrm{i}\boldsymbol{Q} \cdot (\boldsymbol{r}_i(t) - \boldsymbol{r}_j(0)) \right\rangle \tag{5}$$

where b_i is the scattering length of atom i, and $\boldsymbol{r}_i$ is the instantaneous position of atom i. By performing the standard orientational averaging over all directions of $\boldsymbol{Q}$, we obtain

$$F(Q, t) = \sum_{ij} b_i b_j \left\langle \frac{\sin(Q\,\Delta r_{ij}(t))}{Q\,\Delta r_{ij}(t)} \right\rangle \tag{6}$$

where

$$\Delta r_{ij}(t) = |\boldsymbol{r}_i(t) - \boldsymbol{r}_j(0)|. \tag{7}$$

We calculated $F(Q, t)$ for a range of Q, 0–7 Å^{-1}, and for the range of times 0–20 ps. The dynamic structure factor $S(Q, E)$ is the time Fourier transform of $F(Q, t)$ [50]. Because of statistical noise it was necessary to use a Gaussian filter to smooth the data in order to highlight the important overall features. In order to distinguish the molecular dynamics calculation of $S(Q, E)$ we denote it as $S_{\mathrm{MDS}}(Q, E)$

The map of the calculation of $S_{\mathrm{MDS}}(Q, E)$ is shown in figure 16, together with a three-dimensional plot. The map, which is the representation that can most easily be compared with the experimental data of figure 15, shows a broad band of inelastic scattering at just below 4 meV, spread across the range of values of Q, which corresponds to the band of inelastic scattering at 5 meV in the experimental data. This has the same peak, at a value of Q of around 4.5–5 Å^{-1}, as is seen in the experimental data. There is also a peak in the band in $S_{\mathrm{MDS}}(Q, E)$ at a value of Q of around 7 Å^{-1}, which can also be seen on the energy-loss side of the experimental $S(Q, E)$ map. These peaks are highlighted in the three-dimensional plot in figure 16. The band of scattering in $S_{\mathrm{MDS}}(Q, E)$ extends to lower and higher energies, as in the experimental data for silica glass. The map of $S_{\mathrm{MDS}}(Q, E)$ does not highlight the range of values particularly well, and the spread of values of E is better seen in the three-dimensional plot of $S_{\mathrm{MDS}}(Q, E)$ in figure 16.

The calculations of $S_{\mathrm{MDS}}(Q, E)$ show that the simulation sample reproduces the Q–E form of the inelastic scattering reasonably well. It is clear, therefore, that the density-of-states calculations given above (figure 14) do properly represent the behaviour of real materials, and provide confidence in our conclusion that silica glass has a greater degree of flexibility than the crystalline α-cristobalite form of silica. In order to develop the insights further, we now turn to calculations of $S(Q, E)$ for silica glass using the simple split-atom model.

5.4. The dynamic structure factor S(Q, E) from the RUM and CRUSH models

The CRUSH calculations with the split-atom model give both the eigenvalues and eigenvectors of the dynamical matrix, from which the one-phonon inelastic scattering function can

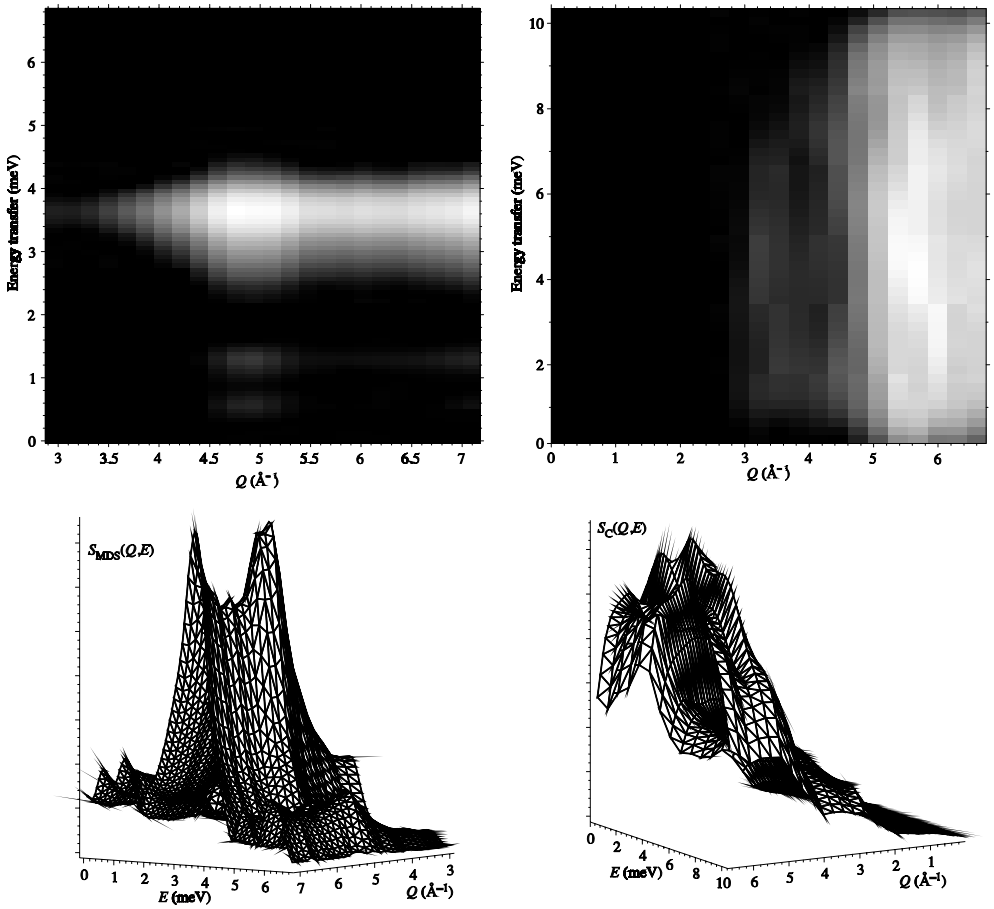

Figure 16. The dynamic structure factor of silica glass, obtained from our molecular dynamics simulation (left, $S_{\mathrm{MDS}}(Q)$) and our split-atom model (right, $S_{\mathrm{C}}(Q)$), shown as intensity maps for comparison with figure 15, and as three-dimensional plots in order to highlight some of the dynamic range of the data.

be calculated. From a classical perspective, the one-phonon scattering function from a mode of wave vector $\boldsymbol{k}$ and label ν at scattering vector $\boldsymbol{Q}$ is given as

$$S_\nu(\boldsymbol{Q}, E) \propto \frac{k_{\mathrm{B}}T}{\omega_\nu^2} \left| \sum_j \boldsymbol{e}(j, \boldsymbol{k}, \nu) \exp(\mathrm{i}\boldsymbol{Q} \cdot \boldsymbol{R}_j) \right|^2 \delta(E \pm \hbar\omega) \tag{8}$$

where $\boldsymbol{e}(j, \boldsymbol{k}, \nu)$ is the polarization vector (mode eigenvector). The overall function $S(\boldsymbol{Q}, E)$ is obtained by summing over all modes for a given value of $\boldsymbol{Q}$:

$$S(\boldsymbol{Q}, E) = \sum_\nu S_\nu(\boldsymbol{Q}, E). \tag{9}$$

In the formalism of the split-atom method, if the sample contains N SiO_4 tetrahedra, there are $6N$ modes for any value of $\boldsymbol{Q}$. We have performed calculations of $S(\boldsymbol{Q}, E)$ for many values of $\boldsymbol{Q}$, and obtained the orientational average $S(Q, E)$ by appropriate binning over ranges of values of Q. We denote the scattering function obtained by this procedure from the split-atom calculations with CRUSH as $S_{\mathrm{C}}(Q, E)$. The map of $S_{\mathrm{C}}(Q, E)$ is shown in figure 16, together with a three-dimensional plot.

The first point to note about the $S_C(Q, E)$ map of figure 16 is that there is more similarity to the experimental and molecular dynamics maps of $S(Q, E)$ and $S_{MDS}(Q, E)$ respectively than is apparent from a quick inspection. There is a band of scattering across the range of values of Q, beginning at around 3 $Å^{-1}$: this band is highlighted in the three-dimensional plot. The CRUSH calculations are tuned (by tuning the force constant of the split-atom spring) so that the maximum energy corresponds to the maximum range of values of energy in quartz below the modes that purely involve Si–O stretching motions. This means that the energy scale on the map has been calibrated against appropriate experimental values and can therefore be compared directly with the experimental and molecular dynamics simulation results. The band of inelastic scattering is centred on 5 meV, similarly to the experimental data, but unlike the case for the experimental data this scattering is very spread out in energy. We also note that there is a peak in $S_C(Q, E)$ at a value of Q of around 5–5.5 $Å^{-1}$, which is highlighted in the three-dimensional plot of figure 16. This reproduces the feature seen in both the experimental $S(Q, E)$ and molecular dynamics $S_{MDS}(Q, E)$ results.

The important point about the CRUSH $S_C(Q, E)$ map of figure 16 is indeed the wide spread of energies. This follows from the same effects as are seen in the CRUSH density-of-states plots, $g_C(\omega)$, where we saw that the existence of the RUMs/floppy modes gave a non-zero value of $g_C(\omega)$ as $\omega \to 0$, but we noted that if more forces were added to the model, then there is a tightening up of the density of states around a non-zero value of ω, but that there remains an excess of low-frequency modes above the normal Debye ω^2-form of $g(\omega)$. The broad band of scattering at 5 meV *is not* directly associated with RUMs/floppy modes, since these are more properly the modes in the limit $\omega \to 0$. Often the boson peak is associated with floppy modes, but this result clearly indicates that the floppy modes are likely to be found at lower energies. In fact, taking all the results of this paper together indicates that the floppy modes will occur over the range of energies between zero and that of the boson peak, appearing as a low-energy tail to the boson peak, exactly as seen in the experimental data and results from the molecular dynamics simulations given in this paper.

6. Summary

Our study of silica glass has addressed several aspects of its low-energy dynamics, namely the dynamics of large-amplitude tetrahedral reorientations and the dynamics of floppy modes. We found that the structure of silica glass can naturally support large-amplitude cooperative reorientations of SiO_4 tetrahedra and identified those motions as responsible for giving rise to two-level tunnelling states in glasses. We have demonstrated by simulating the larger structures of silica glass that it can sustain unexpectedly frequent jump events involving groups of SiO_4 tetrahedra, and, unlike in the small structure simulated previously, jump events happen that are uncorrelated with each other in various parts of the structure. This type of motion, being well represented statistically, can make a considerable contribution to the system's low-energy dynamics and thermal properties.

Comparison of experimental and calculated dynamic structure factors indicates that silica glass is able to support low-ω modes, or rigid unit modes. We have applied the RUM model to larger structures and calculated the vibrational densities of states of silica glass at different temperatures. The RUM analysis, like the analysis of the low-ω spectrum of the vibrational density of states, indicates that silica glass has the same ability to support rigid unit modes as β-cristobalite. The possibility for the glass structure to employ elements of its high-temperature crystalline phase can be explained by these structures having the same RUM flexibility.

Acknowledgments

We acknowledge the kindness of Professor M Thorpe, Michigan State University, in providing the structures of amorphous silicon from which we were able to generate our samples of silica. We are grateful to the EPSRC for financial support, and KT is grateful to the Cambridge Overseas Trust for support. We are also grateful to the staff of ISIS for technical support for obtaining the experimental data. The simulations and calculations were performed using the Hitachi computers of the High Performance Computing Facility in Cambridge.

References

[1] Zeller R C and Pohl R O 1971 *Phys. Rev.* B **4** 2029
[2] Anderson P W, Halperin B I and Varma C M 1972 *Phil. Mag.* **25** 1
[3] Phillips W A 1972 *J. Low Temp. Phys.* **7** 351
[4] Yu C C and Leggett A J 1988 *Comment. Condens. Matter Phys.* **14** 231
[5] Leggett A J 1991 *Physica* B **169** 322
[6] Coppersmith S N 1991 *Phys. Rev. Lett.* **67** 2315
[7] Trachenko K, Dove M T, Hammonds K, Harris M and Heine V 1998 *Phys. Rev. Lett.* **81** 3431
[8] Thorpe M F 1983 *J. Non-Cryst. Solids* **57** 355
[9] Thorpe M F, Djordjevic B R and Jacobs D J 1997 *Amorphous Insulators and Semiconductors (NATO ASI Series)* ed M F Thorpe and M I Mitkova (Dordrecht: Kluwer) p 289
[10] Dove M T, Harris M J, Hannon A C, Parker J M, Swainson I P and Gambhir M 1997 *Phys. Rev. Lett.* **78** 1070
[11] Foret M, Courtens E, Vacher R and Suck J B 1996 *Phys. Rev. Lett.* **77** 383
[12] Taraskin S N and Elliott S R 1997 *Phys. Rev.* B **56** 8605
[13] Hammonds K D, Dove M T, Giddy A P, Heine V and Winkler B 1996 *Am. Mineral.* **81** 1057
[14] Dove M T, Hammonds K D, Harris M J, Heine V, Keen D A, Pryde A K A, Trachenko K O and Warren M C 2000 *Mineral. Mag.* **64** 377
[15] Giddy A P, Dove M T, Pawley G S and Heine V 1993 *Acta Crystallogr.* A **49** 697
[16] Dove M T, Heine V and Hammonds K D 1995 *Mineral. Mag.* **59** 629
[17] Dove M T, Trachenko K O, Tucker M G and Keen D A 2000 *Rev. Mineral.* at press
[18] Gaskell P H and Wallis D J 1996 *Phys. Rev. Lett.* **76** 66
[19] Keen D A and Dove M T 1999 *J. Phys.: Condens. Matter* **11** 9263
[20] Keen D A and Dove M T 2000 *Mineral. Mag.* **64** 447
[21] Wright A C 1994 *J. Non-Cryst. Solids* **179** 84
[22] Keen D A 1997 *Phase Transitions* **61** 109
[23] Vessal B, Amini M and Catlow C 1993 *J. Non-Cryst. Solids* **159** 184
[24] Evans D L and King S V 1966 *Nature* **212** 1353
[25] Bell R J and Dean P 1972 *Phil. Mag.* **25** 1381
[26] Wooten F, Winer K and Weaire D 1985 *Phys. Rev. Lett.* **54** 1392
[27] Wooten F and Weaire D 1987 *Solid State Physics* vol 40 (New York: Academic) p 1
[28] Tsuneyuki S, Tsukada M, Aoki H and Matsui Y 1988 *Phys. Rev. Lett.* **61** 869
[29] Smith W and Forester T 1996 *J. Mol. Graph.* **14** 136
[30] Guttman L J and Rahman S M 1986 *Phys. Rev.* B **33** 1506
[31] Smith D A 1979 *Phys. Rev. Lett.* **42** 729
[32] Harris R and Lewis L J 1982 *Phys. Rev.* B **25** 4997
[33] Weber T A and Stillinger F H 1985 *Phys. Rev.* B **32** 5402
[34] Heuer A and Silbey R J 1993 *Phys. Rev. Lett.* **70** 3911
[35] van Ee L D, Thijsse B J and Sietsma J 1997 *Mater. Sci. Eng.* A **226–228** 296
[36] van Ee L D, Thijsse B J and Sietsma J 1997 *Phys. Rev.* B **57** 906
[37] Buchenau U, Prager M, Nücker N, Dianoux A J, Ahmad N and Phillips W A 1986 *Phys. Rev.* B **34** 5665
[38] Buchenau U, Zhou H M, Nücker N, Gilroy K S and Phillips W A 1988 *Phys. Rev. Lett.* **60** 1318
[39] Maxwell J C 1864 *Phil. Mag.* **27** 294
[40] Pryde A K A, Hammonds K D, Dove M T, Heine V, Gale J D and Warren M C 1996 *J. Phys.: Condens. Matter* **8** 10 973
[41] Welche P R L, Heine V and Dove M T 1998 *Phys. Chem. Minerals* **26** 63
[42] Heine V, Welche P R L and Dove M T 1999 *J. Am. Ceram. Soc.* **82** 1793

[43] Hammonds K D, Deng H, Heine V and Dove M T 1997 *Phys. Rev. Lett.* **78** 3701
[44] Hammonds K D, Heine V and Dove M T 1998 *J. Phys. Chem.* B **102** 1759
[45] Dove M T, Gambhir M and Heine V 1999 *Phys. Chem. Minerals* **26** 344
[46] Hammonds K D, Dove M T, Giddy A P and Heine V 1994 *Am. Mineral.* **79** 1207
[47] Hammonds K D, Bosenick A, Dove M T and Heine V 1988 *Am. Mineral.* **83** 476
[48] Swainson I P and Dove M T 1993 *Phys. Rev. Lett.* **71** 3610
[49] Harris M J, Dove M T and Parker J M 2000 *Mineral. Mag.* **64** 435
[50] Dove M T 1993 *Introduction to Lattice Dynamics* (Cambridge: Cambridge University Press)
[51] Swainson I P and Dove M T 1995 *J. Phys.: Condens. Matter* **7** 1771
[52] Bermejo F J, Cabrillo C, Dove M T, Tucker M G, Trachenko K O, Keen D A, Harris M J and Bennington S M 2000 *Phys. Rev. Lett.* submitted